Journal of Metals, Materials and Minerals, 35(1), e2148, 2025

Arginine-modified surface coffee grounds activated carbon for Pb^{2+} adsorption: Kinetic, isotherm and thermodynamic studies

Jarawee CHUPIROM[1], Sirikorn KHAOPHONG[1], Nopporn HEMYAKORN[1], Sonchai INTACHAI[1,2], and Panita KONGSUNE[1,2,*]

[1] *Department of Chemistry, Faculty of Science and Digital Innovation, Thaksin University, Phattalung, 93210, Thailand*
[2] *Innovative Material Chemistry for Environment Center, Thaksin University, Phattalung, 93210, Thailand*

***Corresponding author e-mail**: dpanita@tsu.ac.th

Received date:
10 September 2024
Revised date:
3 December 2024
Accepted date:
18 December 2024

Keywords:
Lead;
Arginine;
Adsorption;
Desorption;
Activated carbon

Abstract

This research focuses on enhancing the value of coffee waste by converting it into activated carbon for removing Pb^{2+} ions from contaminated water. Coffee grounds were activated with KOH and carbonized at 600°C for 4 h to produce activated carbon (CGAC), then modified with arginine via hydrothermal treatment at 120°C for 48 h to create Arg-CGAC. The adsorbents' chemical and physical properties were analyzed using SEM, FT-IR, BET, and pH_{pzc} methods. Batch experiments revealed that Arg-CGAC exhibited superior Pb^{2+} adsorption (223.10 $mg{\cdot}g^{-1}$) compared to CGAC (119.23 $mg{\cdot}g^{-1}$) under optimal conditions. Isotherm analysis showed stronger adsorbate-adsorbent interactions and a more endothermic adsorption for Arg-CGAC. Arg-CGAC demonstrated both physisorption and weak chemisorption, while CGAC primarily exhibited physisorption. Increasing temperatures made $\Delta G°$ values more negative, indicating more favorable adsorption for Arg-CGAC. Desorption tests showed a 98% yield over four cycles, but efficiency declined after the 7th cycle, stabilizing at 55% to 60%, suggesting good initial performance despite some regeneration limitations.

1. Introduction

Lead is a highly toxic heavy metal that poses significant risks to human health and the environment. It contaminated water through various sources such as battery manufacturing, agricultural chemicals, and industrial waste. This contamination disrupts plant growth, introduces toxins into the food chain, and harms the health of living organisms, especially children and pregnant women, who are particularly vulnerable to lead exposure. Even at low levels, lead can cause developmental delays, learning difficulties, and cognitive impairments, while higher levels can lead to severe neurological, renal, and cardiovascular damage.

Addressing lead contamination is crucial for protecting both public health and the environment. Researchers have explored various methods to remove lead from contaminated sites, including chemical treatments [1,2] and more sustainable approaches [3,4]. Among the most promising methods for mitigating lead pollution is the use of adsorbents materials that can bind and remove lead ions from contaminated water. Adsorbents have gained attention due to their efficiency, cost-effectiveness, and versatility in addressing lead contamination across different environmental settings. Natural materials like clays [5], zeolites [6,7], biochars [8], and synthetic materials such as activated carbon [9] and nanomaterials [3] have been studied for their ability to bind and remove lead ions from the environment. These materials work by adsorbing lead ions onto their surfaces, thereby reducing the concentration of lead in the environment. Research has shown that, depending on the type and modification of the adsorbent, it is possible to achieve high removal efficiencies even in environments with complex contamination profiles. Among the various methods explored for mitigating this issue, the use of activated carbon has emerged as a particularly effective and versatile solution. Activated carbon, known for its high surface area and adsorption capacity, has been widely studied for its ability to remove lead ions from contaminated water.

Activated carbon, in particular, has emerged as a highly effective solution. Produced from organic materials like wood, coconut shells, and agricultural waste, it is a sustainable and cost-effective option for environmental remediation [10,11]. Its porous structure enables it to trap and retain lead particles, significantly reducing lead concentrations in contaminated water and soil [9,12-14]. Coffee waste is generated in ton volumes and its inherent chemical structural groups have elicited interest from researchers to investigate it for developing low-cost adsorbents for heavy metal removal [10,15-17]. The review shows that using low-cost adsorbents is eco-friendly, cost-effective, and is a simple technique for water and wastewater treatment containing Pb^{2+} ions. However, gaps exist to increase adsorption ability. Furthermore, advancements in modifying activated carbon, such as adding functional groups or incorporating metal oxides, have enhanced its ability to remove lead more efficiently.

Various studies have explored the functionalization of activated carbon to improve its metal adsorption capacity [18]. Carboxyl groups functionalized activated carbon enhance the adsorption of Pb^{2+} through ion exchange and complexation mechanisms [18]. The study reported that carboxyl-functionalized AC showed an increase in Pb^{2+} adsorption capacity by up to 30% compared to unmodified AC. Amino Groups ($–NH_2$): Amino-functionalized activated carbon has also been extensively

studied [19-21] found that the introduction of amino groups on AC significantly improved Pb^{2+} adsorption due to the formation of strong coordination bonds between Pb^{2+} ions and nitrogen atoms in the amino groups. The study reported a 40% increase in adsorption capacity compared to non-functionalized AC. The study by Liu *et al.* (2015) [22] suggested that amino groups were more effective than carboxyl and hydroxyl groups, with the highest Pb^{2+} adsorption capacity observed for amino-functionalized AC.

This research aims to explore and enhance the effectiveness of activated carbon in lead removal by functionalizing it with arginine, a basic amino acid with a guanidino group. Arginine offers multiple interaction sites [19-21] for Pb^{2+} ions, potentially increasing the adsorption capacity of activated carbon. This study also seeks to correlate the treatment methods of arginine-modified and unmodified coffee ground activated carbon adsorbents with their adsorption efficiency. Additionally, we will investigate adsorption conditions, isotherms, kinetics, and thermodynamics to develop a practical adsorbent that enhances the value of waste materials and reduces environmental impact.

2. Methodology

2.1 Chemicals and reagents

The coffee grounds used in this study were sourced from Thaksina Café, Thaksin University, Phatthalung Province, Thailand. L-Arginine ($C_6H_{14}O_2$; purity 99%) was obtained from Himedia. Lead (II) nitrate ($Pb(NO_3)_2$; purity ≥99%), potassium hydroxide (KOH; purity 85%), and hydrochloric acid (HCl; purity 36%) were obtained from Elago Enterprises Pty Ltd. The Nafion™ 117 solution ($C_7HF_{13}O_5S{\circ}C_2F_4$; purity 5 wt%) was acquired from Sigma-Aldrich Pty Ltd. All solvents used, including ethanol (C_2H_6O; purity 99.8%) was purchased from E. Merck.

2.2 Preparation of GCAC and Arg-CGAC

Coffee grounds were initially dried at 105°C for 24 h to remove moisture. The dried coffee grounds were then mixed with 85% potassium hydroxide and water in a 1:1:2 weight ratio and thoroughly stirred. The mixture was incubated at room temperature for 24 h before being transferred to a crucible and heated in a furnace at 600°C for 4 h. After cooling, the activated carbon was neutralized using 0.1 M hydrochloric acid until a neutral pH was achieved, rinsed with distilled water, and dried again at 105°C for 24 h. The final product is referred to as CGAC.

For the preparation of arginine-modified activated carbon (Arg-CGAC) via hydrothermal treatment, 1 g of activated carbon was mixed with 2 g of arginine and 15 mL of water. The mixture was thoroughly mixed and then placed in a hydrothermal reactor, where it was heated at 120°C for 48 h. After cooling, the product was rinsed with water and dried at 105°C for 24 h to remove moisture. The resulting samples are designated as Arg-CGAC.

2.3 Characterization of GCAC and Arg-CGAC

The morphology of the adsorbents was examined using a Field Emission Instruments Environmental Scanning Electron Microscope (FESEM Quanta 450 FEG Switzerland). Elemental mapping and distribution were analyzed using Energy Dispersive Spectroscopy. Surface functional groups were investigated using a Fourier Transform Infrared (FTIR) Spectrometer (ATR-FTIR; G8044AA, Agilent Technologies) in the range of 650 cm^{-1} to 4000 cm^{-1}. The porous texture of the activated carbons was characterized using N_2 adsorption/desorption isotherms at 77 K, measured with a nitrogen sorption instrument (Quantachrome Autosorb-iQ2-MP, USA). Surface area was determined via the Brunauer-Emmett-Teller (BET) method, and pore size distribution was obtained using the Barrett-Joyner-Halenda (BJH) method. Phase structure was verified through Powder X-ray diffraction (XRD) analysis, utilizing a Bruker D8 ADVANCE diffractometer and a PAN analytical Empyrean powder diffractometer.

To estimate surface acidity, 0.20 g of each sample was mixed with 25 mL of 0.05 M NaOH solution in a conical flask and left for 48 h at room temperature. The mixtures were then separated, and the filtrates were titrated using 0.05 M HCl solution. Similarly, surface basicity was determined by mixing 0.20 g of each adsorbent with 25 mL of 0.05 M HCl solution, left for 48 h, and titrated using 0.05 M NaOH.

2.4 Batch adsorption experiments

The adsorption capacity of GCAC and Arg-CGAC for Pb^{2+} removal from aqueous solutions was investigated under various conditions. The study examined the effects of adsorbent dosage, initial Pb^{2+} concentration, contact time, and temperature on adsorption equilibrium. To optimize these parameters, adsorption experiments were conducted using GCAC and Arg-CGAC soaked in 200 mL of 100 $mg{\cdot}L^{-1}$ Pb^{2+} solution at 30°C for 60 min in a shaker bath set to 240 rpm. Different adsorbent dosages ranging from 0.10 g to 0.50 g were tested with 150 mL of Pb^{2+} solutions at initial concentrations varying from 5 $mg{\cdot}L^{-1}$ to 100 $mg{\cdot}L^{-1}$. Contact times ranged from 15 min to 180 min, and experiments were performed at temperatures between 30°C and 50°C, also in a shaker bath set to 240 rpm. The initial and final concentrations of Pb^{2+} in the solution were analyzed using inductively coupled plasma optical emission spectroscopy (ICP-OES). The adsorption capacity at equilibrium (q_e) in $mg{\cdot}g^{-1}$ unit was calculated as Equation (1). While the percentage of Pb^{2+} removed from the solution (% removal) was calculated using Equation (2).

$$q_e = \left(\frac{C_0 - C_e}{W}\right) \times V \quad (1)$$

$$\% \text{ Adsorption} = \left(\frac{C_0 - C_e}{C_0}\right) \times 100 \quad (2)$$

Where C_0 and C_e are the initial and equilibrium concentrations ($mg{\cdot}L^{-1}$) of Pb^{2+} solution while W, and V are mass of adsorbents (g) and volume of the solution (L), respectively.

3. Results and discussion

3.1 Characteristics of adsorbents

Understanding the acidic and basic properties of activated carbon is crucial for an effective adsorption process and their acidic and basic data were listed in Table 1. The raw coffee grounds (CG) exhibit

the highest acidic properties at 1.23 mmol·g^{-1}, primarily due to the presence of oxygen-containing functional groups, while the basic properties are lower at 0.90 mmol·g^{-1}. After activation and carbonization at high temperatures to produce CGAC, the acidic properties decrease to 0.39 mmol·g^{-1}, and the basic properties increase to 1.27 mmol·g^{-1} due to the reduction of oxygen-containing groups. When CGAC is modified with arginine, the acidic properties increase to 0.58 mmol·g^{-1}, and the basic properties reach their highest level at 1.35 mmol·g^{-1} due to the introduction of nitrogen- and oxygen-containing compounds.

The adsorption capacity is generally related to the specific surface area and pore volume of the adsorbents. The pore volume affects the size of adsorbed molecules, while the surface area influences the quantity of adsorbed molecules. The BET method was employed to investigate the porous structure parameters of the adsorbents. The BET surface area (S_BET, m^2·g^{-1}), total pore volume (V_T, cm^3·g^{-1}), and average pore diameter (nm) of CGAC and Arg-CGAC are listed in Table 1. Compared to CG and Arg-CGAC, CGAC exhibited the highest BET surface area, with values of 470.61 m^2·g^{-1}, whereas the BET surface areas for CG and Arg-CGAC were 3.25 m^2·g^{-1} and 301.68 m^2·g^{-1}, respectively. The average pore diameter of Arg-CGAC was larger than that of CGAC. The significant decrease in BET surface area and pore volume after modification with arginine, along with the increase in average pore diameter, can be attributed to structural changes caused by the entrapment of arginine in the pores. This modification resulted in the formation of wider pores and a more basic surface, as nitrogen interacted with carbonyl groups (–COH) on the AC surface.

The EDS analysis provided the elemental composition of CG, CGAC, and Arg-CGAC (Table 1). Carbon (C) and oxygen (O) were the main components in all samples. The CG sample contained 76.41% C, 2.25% N, and 21.48% O. In CGAC, the composition was 82.70% C, 1.66% N, and 15.00% O, while in Arg-CGAC, it was 72.70% C, 25.57% N, and 16.56% O. The higher carbon and lower oxygen content in CGAC suggests increased graphitization and the removal of volatile compounds during carbonization. The highest nitrogen content in Arg-CGAC indicates successful arginine modification, leading to the formation of nitrogen and oxygen functional groups on the CGAC surface.

SEM images of the CGAC and Arg-CGAC adsorbents were captured to visualize their surface structures, as shown in Figure 1. The CGAC sample, produced through a one-step process involving KOH impregnation at room temperature for 24 h followed by carbonization at 600°C for 4 h, exhibited a highly porous structure. In comparison, the surface morphology of the Arg-CGAC sample, which was modified with arginine, revealed a significantly more cracked and open pore structure, particularly on the surface. This indicates that the arginine modification effectively altered the surface characteristics of the CGAC, enhancing the formation of open and accessible pores. These results suggest that arginine modification had a noticeable impact on the surface morphology of CGAC, potentially contributing to improved adsorption properties.

The surface functional groups of the adsorbents play a crucial role in their adsorption capacity. To verify the changes in surface functional groups before and after carbonization and arginine doping on CGAC, Fourier-transform infrared (FTIR) spectroscopy was performed on CG, CGAC, and Arg-CGAC, with the results shown in Figure 2(a). The FTIR spectrum of the raw coffee grounds (CG) displayed the most functional groups among the samples. The broad absorption band in the range of 3600 cm^{-1} to 3200 cm^{-1} corresponds to O-H stretching, indicative of moisture and hydroxyl (–OH) groups in the sample. Peaks at 2922, 2854, 1365, and 1317 cm^{-1} are associated with aliphatic C-H stretching, while the peak at 1155 cm^{-1} suggests the presence of C-C bonds. The prominent peaks at 1625 cm^{-1} and 1030 cm^{-1} are attributed to C=C and C-O stretching, respectively, with the peak at 896 cm^{-1} indicating the presence of C-O-H groups [9,11]. After carbonization to produce CGAC, the FTIR spectrum exhibited a new band at 2360 cm^{-1}, attributed to C≡C vibrations in alkyne groups, which was more intense due to the release of volatile matter during carbonization. The peaks around 1571 cm^{-1} and 1544 cm^{-1} could be associated with C=C stretching of aromatic rings and carboxylic acids.

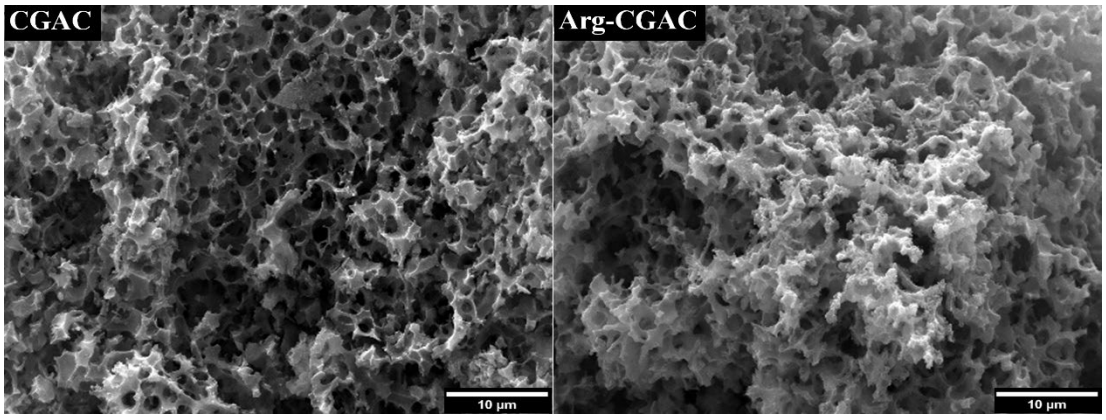

Figure 1. The SEM photographs of CGAC and Arg-CGAC adsorbents.

Table 1. The acidic and basic values, surface arears, and the %atomic by EDS of CG, CGAC and Arg-CGAC adsorbents.

Adsorbents	Acidic basic site [mmol·g^{-1}]	Surface arears [m^2·g^{-1}]	Pore volume [cm^3·g^{-1}]	Pore diameter [nm]	Adsorbents	%Atomic			
						C	N	O	Others
CG	1.23	0.9	3.25	-	-	76.41	2.25	21.08	0.26
CGAC	0.39	1.27	470.61	0.27	2.40	82.70	1.66	15.00	0.64
Arg_CGAC	0.58	1.35	301.68	0.16	13.90	72.86	25.57	16.56	5.01

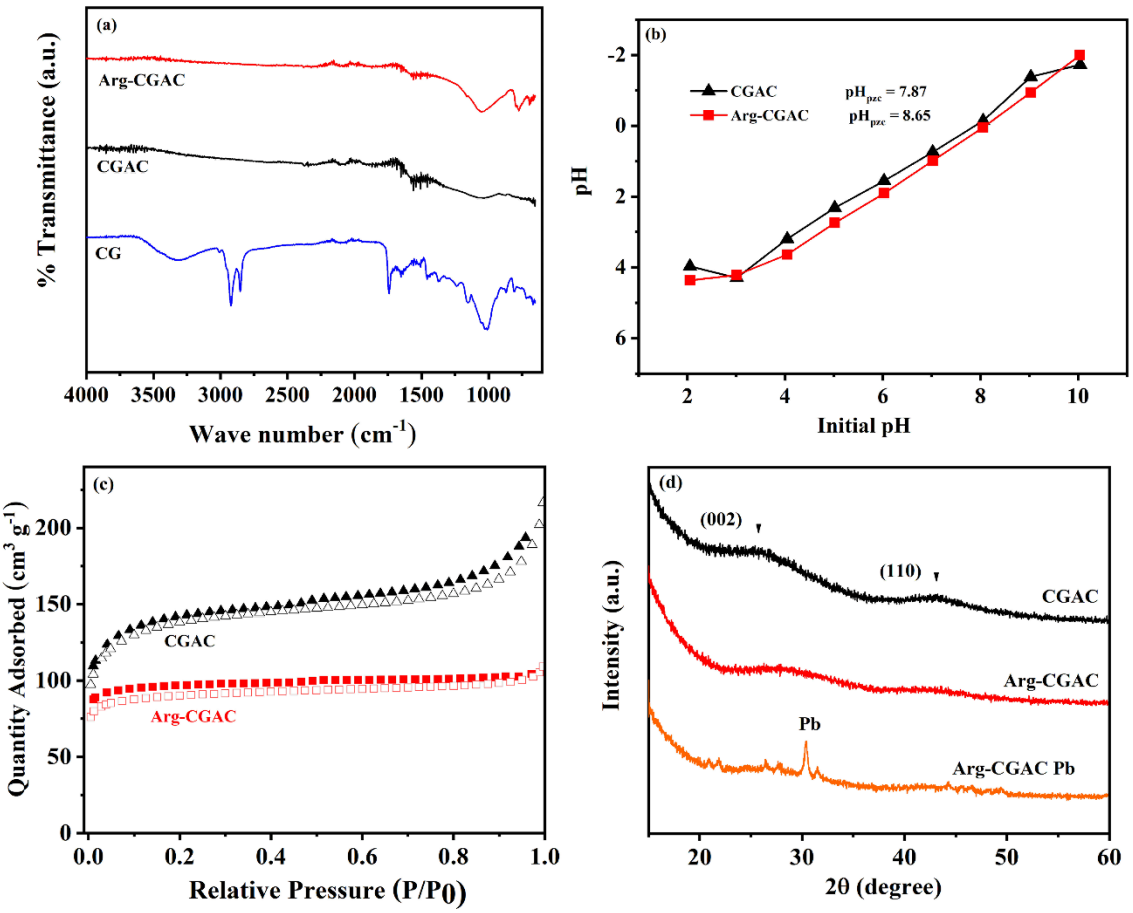

Figure 2. The (a) FTIR spectra, (b) pH_{pzc} of adsorbents, (c) nitrogen adsorption-desorption isotherm plot, and (d) XRD pattern.

A band at lower frequencies (~750 cm^{-1}) indicates the presence of potassium, suggesting that heat treatment disrupts the cellulose or hemicellulose structure in coffee grounds. Upon arginine modification (Arg-CGAC), the C-O/C-N stretching peak at 1000 cm^{-1} to 1300 cm^{-1} is retained with increased intensity compared to CGAC. Additionally, peaks in the 800 cm^{-1} to 900 cm^{-1} range, attributed to out-of-plane bending or deformation of C-H/N-H in the guanidino group (-C(=NH)-NH_2), confirm the successful grafting of arginine onto the CGAC surface [23].

The point of zero charge (pH_{pzc}) is a critical parameter in surface chemistry, representing the pH at which a material's surface carries no net electrical charge. The pHpzc values for CGAC and Arg-CGAC were determined to be 7.87 and 8.65, respectively, as shown in Figure 2(b). At pH levels below these values, the adsorbent surfaces tend to be negatively charged, enhancing their ability to attract Pb^{2+} ions. Conversely, at pH levels above 7.87 for CGAC and 8.65 for Arg-CGAC, the surfaces become positively charged, reducing their affinity for Pb^{2+} ions. This parameter is essential for understanding the adsorption interactions between Pb^{2+} and the adsorbents in aqueous solutions.

Adsorption isotherms provide insight into the surface area, pore volume, and porous structure of adsorbents. According to the International Union of Pure and Applied Chemistry (IUPAC) classification, gas physisorption isotherms are categorized into six types, with the first five types suggested by Brunauer *et al.* (1938) [24]. The nitrogen adsorption-desorption isotherms for CGAC and Arg-CGAC, plotted in Figure 2(c), exhibit similarities in shape, corresponding to Type I and IV isotherms. This indicates a mixed microporous and mesoporous structure, characteristic of effective adsorbents.

The X-ray diffraction (XRD) patterns of CGAC, Arg-CGAC, and Arg-CGAC after Pb^{2+} adsorption are shown in Figure 2(d). Activated carbon typically lacks a well-defined crystalline structure, leading to a broad peak centered around 2θ values of approximately 20° to 30° in its XRD pattern. This broad peak is indicative of disordered or amorphous carbon. In Figure 2(d), the XRD patterns of CGAC and Arg-CGAC display peaks around 24° and 43°, corresponding to a graphitic-like structure of activated carbon, suggesting a degree of graphitization that enhances electrical conductivity. After Pb^{2+} adsorption, the XRD pattern of Arg-CGAC shows a new peak around 31°, corresponding to the presence of Pb atoms [25].

3.2 Influence of dose, concentration, time, and temperature on Pb^{2+} adsorption

The influence of adsorbent dose, concentration of Pb^{2+} solution, contact time, and temperature on Pb^{2+} adsorption by CGAC and Arg-CGAC were shown in Figure 3(a-d). The adsorption of Pb^{2+} ions was systematically studied by varying the amount of CGAC adsorbent (0.1 g to 0.5 g) at a Pb^{2+} concentration of 100 $mg{\cdot}L^{-1}$, with a contact time of 90 min, and a temperature of 30°C. The results indicated that the amount of Pb^{2+} adsorbed per unit weight of adsorbent at time t (q_t) decreased as the adsorbent dose increased (Figure 2(a)).

Specifically, the maximum adsorption capacity (q_e) of Pb^{2+} ions was 171.92 mg·g^{-1} with 0.1 g of CGAC. This capacity decreased to 67.75 mg·g^{-1} and 31.24 mg·g^{-1} when 0.25 g and 0.50 g of CGAC were used under the same conditions. At lower dosages, the adsorbent particles are more efficiently dispersed, ensuring better accessibility of active sites for Pb^{2+} ions. However, as the dosage increases, overlapping or aggregation of adsorbent particles can occur, reducing the effective surface area and the number of available active sites. Additionally, the increase in adsorbent dosage results in a lower Pb^{2+} concentration per unit mass of adsorbent, leading to a reduced driving force for the mass transfer of Pb^{2+} ions to the adsorbent surface. Based on these findings, adsorbent dosages of 0.1 g and 0.25 g were selected for further studies to compare the effect of Pb^{2+} concentration on CGAC and Arg-CGAC.

Subsequent experiments revealed that the adsorption capacities of both CGAC and Arg-CGAC increased as the initial Pb^{2+} concentration rose from 10 mg·L^{-1} to 150 mg·L^{-1} (Figure 3(b)). Both adsorbents (0.1 g adsorbents, 150 mg·g^{-1} Pb^{2+}) reached adsorption equilibrium within 90 min (Figure 3(c)), after which no significant changes in adsorption capacity were observed. The adsorption process for both materials (0.1 g adsorbents, 150 mg·L^{-1} $Pb^{2+}$and 90 min contact time) was found to be endothermic (Figure 3(d)), suggesting that increasing the temperature could enhance the adsorption capacity.

Notably, Arg-CGAC exhibited a significantly higher Pb^{2+} adsorption capacity compared to CGAC. The maximum q_e values for Arg-CGAC and CGAC were 223.10 mg·g^{-1} and 199.23 mg·g^{-1}, respectively, under identical conditions (0.1 g adsorbent, 150 mg·L^{-1} Pb^{2+}, 90 min contact time, 30°C). This enhancement in adsorption capacity is attributed to the presence of amino and carboxyl functional groups in arginine, which provide multiple interaction sites for Pb^{2+} ions.

3.3 Adsorption kinetics

To understand the behavior of adsorbents and study the mechanisms controlling adsorption, kinetic models have been proposed and experimental kinetic data plotted was displayed in Figure 4(a-b). The adsorption of Pb^{2+} ions was investigated over a contact time range of 0 min to 150 min, using 0.1 g of adsorbent at a Pb^{2+} concentration of 150 mg·L^{-1} and a temperature of 30°C. The pseudo-first-order rate equation in linear form is the first model used to analyze the adsorption rate of the sorbent and is given as Equation (3) while the pseudo-second-order model is given as Equation (4). The adsorption kinetics of Pb^{2+} onto CGAC and Arg-CGAC adsorbents were found to follow the pseudo-second-order kinetic model (Figure 4(b)), as indicated by higher R^2 values compared to the pseudo-first-order model (Figure 4(a)). The experimental q_e values for CGAC and Arg-CGAC were 199.23 mg·g^{-1} and 223.10 mg·g^{-1}, closely matching the theoretical q_e values of 200.01 mg·g^{-1}and 222.05 mg·g^{-1}, respectively (Table 2), demonstrating the model's accuracy.

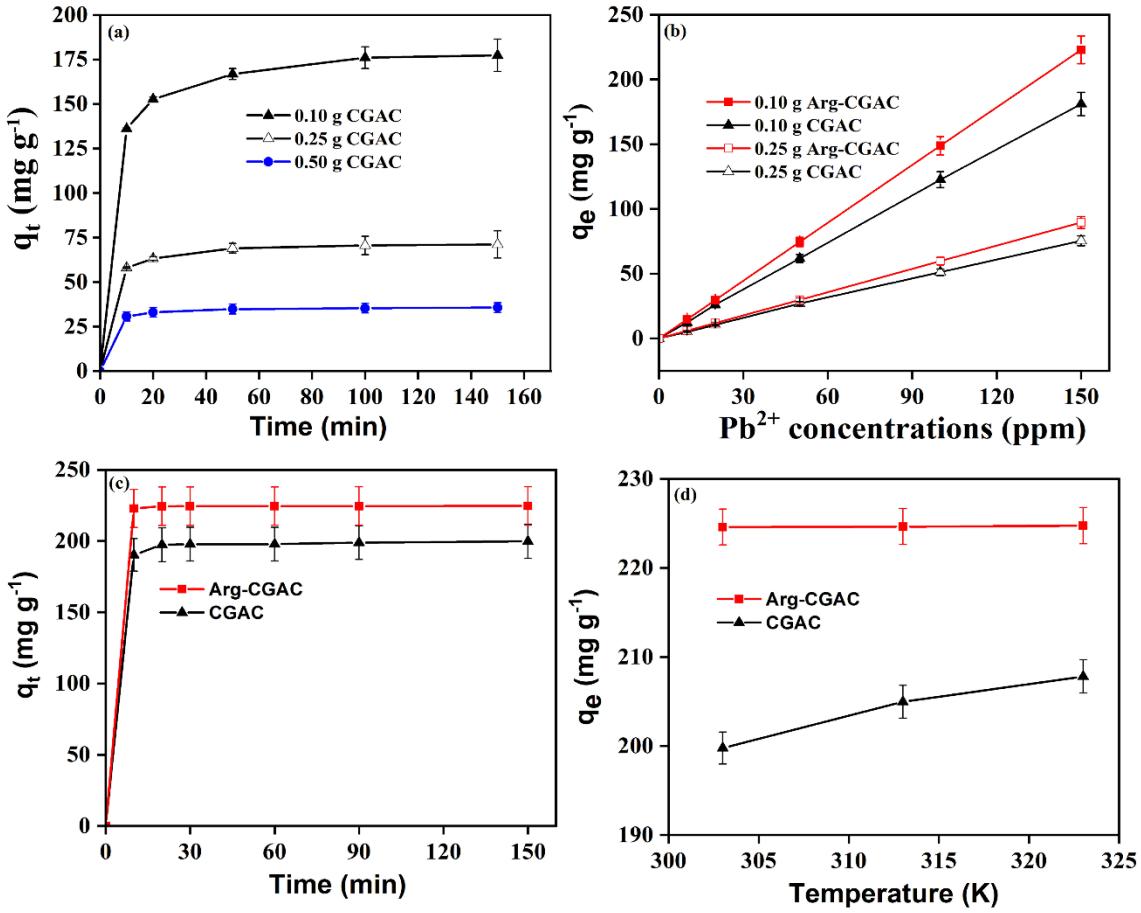

Figure 3. The effects of (a) adsorbent dosage, (b) initial solution concentration, (c) contact time, and (d) temperature on Pb^{2+} adsorption capacity by CGAC and Arg-CGAC adsorbents.

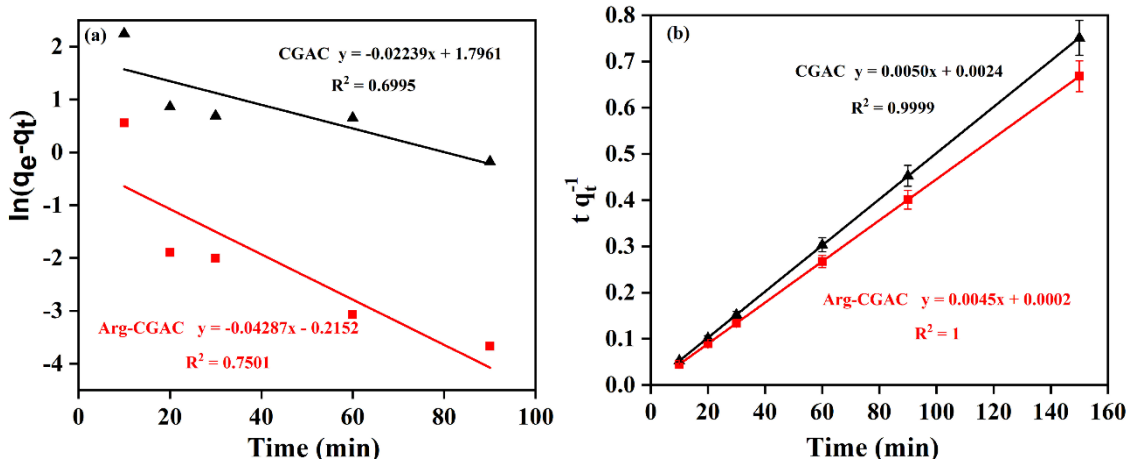

Figure 4. Kinetics plots of (a) pseudo-first-order, and (b) pseudo-second-order on Pb^{2+} adsorption capacity by CGAC and Arg-CGAC adsorbents.

Table 2. Parameters of the kinetic pseudo-first-order, pseudo-second-order of CGAC and Arg-CGAC adsorbents on Pb^{2+} ion adsorption.

Adsorbents	$q_{e(exp)}$ [mg·g^{-1}]	Pseudo-first order $\ln(q_e - q_t) = \ln q_e - k_1 t$ …(3)			Pseudo-second order $\frac{1}{q_t} = \frac{1}{k_2 q_e^2} + \frac{t}{q_e}$ …(4)		
		$q_{e(cal)}$ [mg·g^{-1}]	K [min^{-1}]	R^2	$q_{e(cal)}$ [mg·g^{-1}]	K [min^{-1}]	R^2
CGAC	199	6.03	0.0224	0.6995	200	0.01	0.9999
Arg-CGAC	233	0.81	0.0429	0.7501	222	0.10	1.000

Table 3. Parameters of the Langmiur, Freundlich, Temkin and Dubinin–Radushkevich (D-R) isotherms for CGAC and Arg-CGAC adsorbents on Pb^{2+} ion adsorption.

Model/Equation	Parameters	CGAC	Arg-CGAC
Langmuir $\frac{C_e}{q_e} = \frac{1}{q_m K_L} + \frac{C_e}{q_m}$ ….. (5)	K_L(L·mg^{-1})	0.22	0.87
	q_m (mg·g^{-1})	102.04	250.00
	R^2	0.9355	0.9067
Freundlich $\ln q_e = \ln K_F + \frac{1}{n} \ln C_e$ ….. (6)	K_F (L·mg^{-1})	8.64	186.64
	N	1.10	0.79
	R^2	0.9846	0.9397
Temkin $q_e = B_1 \ln k_T + B_1 \ln C_e$ ….. (7)	K_T (L·mg^{-1})	0.57	6.01
	B_1	56.22	103.12
	R^2	0.9214	0.9625
D-R $E = \frac{1}{\sqrt{2K_D}}$ ….. (8)	K_D (L·mg^{-1})	1.97	0.13
	E	0.50	1.96
	R^2	10.8871	00.9266
When *** $\ln q_e = \ln q_m - K_D \varepsilon^2$ ….. (9), $\varepsilon = RT \ln(1 + \frac{1}{C_e})$ ….. (10)			

3.4 Adsorption isotherms

Adsorption isotherms describe the specific relationship between the adsorption capacity and the concentration of the remaining adsorbate at a constant temperature. The two most commonly used models are the Freundlich and Langmuir isotherms. The Langmuir isotherm assumes monolayer sorption [26], while the Freundlich isotherm accounts for heterogeneous surface energies and multilayer adsorption [27]. Additionally, the Temkin isotherm, which considers the heat of adsorption due to adsorbate-adsorbent interactions [28], was also examined. This model is often applied to chemical adsorption on solid adsorbents and liquid adsorbates. Furthermore, the Dubinin-Radushkevich (D-R) isotherm was used to evaluate whether the adsorption of Pb^{2+} onto CGAC and Arg-CGAC is physical or chemical in nature [29].

The Freundlich, Langmuir, Temkin, and D-R isotherm plots for Pb^{2+} adsorption onto CGAC and Arg-CGAC are shown in Figure 5 (a-d), respectively, with corresponding parameters in Table 3. The R^2 values were used to assess the fit of each isotherm model. The Langmuir isotherm describes monolayer adsorption, and the slightly lower R^2 value for Arg-CGAC suggests a slightly weaker fit to this model compared to CGAC, though both fit reasonably well (Figure 5(a)). The maximum adsorption capacity (q_m) for Arg-CGAC (250.00 mg·g^{-1}) is much higher than for CGAC (102.04 mg·g^{-1}), indicating Arg-CGAC's greater capacity to adsorb Pb^{2+} per unit mass. The higher Langmuir constant (K_L) for Arg-CGAC also suggests a stronger affinity for Pb^{2+}. The Freundlich isotherm fit the CGAC data better, with a higher R^2 value, indicating multilayer adsorption on heterogeneous surfaces (Figure 5(b)). The adsorption capacity constant (K_F) is significantly higher for Arg-CGAC, showing its stronger adsorption capacity for

Pb^{2+}. The n value reflects adsorption intensity; for CGAC, n=1.10 suggests favorable adsorption, while n=0.79 for Arg-CGAC indicates weaker adsorption at lower concentrations.

The Temkin and D-R isotherms also fit the data well for Arg-CGAC (Figure 5(c)). The Temkin constant (K_T) is much higher for Arg-CGAC, indicating stronger adsorbate-adsorbent interactions. The B1 value, which relates to the heat of adsorption, is also higher for Arg-CGAC, suggesting a more endothermic adsorption process compared to CGAC. The D-R isotherm helps distinguish between physisorption and chemisorption based on the E value (Figure 5(d)). For CGAC, E=0.50 $kJ \cdot mol^{-1}$ indicates physisorption, driven by weak van der Waals forces. For Arg-CGAC, E=1.96 $kJ \cdot mol^{-1}$ is closer to the chemisorption range, suggesting a possible combination of physisorption and weak chemisorption.

In conclusion, the isotherm results suggest that Arg-CGAC has a higher adsorption capacity, stronger adsorbate-adsorbent interactions, and a more endothermic adsorption process compared to CGAC. Arg-CGAC's adsorption behavior involves both physisorption and weak chemisorption, while CGAC predominantly exhibits physisorption. The Freundlich and Temkin isotherms provide the best fit for both materials, with Arg-CGAC showing a particularly strong affinity for Pb^{2+}.

3.5 Adsorption thermodynamics

In addition to adsorption kinetics and equilibrium isotherms, thermodynamic parameters such as Gibbs free energy (ΔG°), enthalpy (ΔH°), and entropy (ΔS°) are crucial for understanding the adsorption process. The effect of temperature on Pb^{2+} sorption was studied at 303, 313, and 323 K. Results showed that the removal efficiency of Pb^{2+} increased with rising temperature, indicating an endothermic process. The thermodynamic parameters, presented in Table 4, revealed negative ΔG° values, confirming the spontaneous and feasible nature of the adsorption. The ΔG° values became more negative with increasing temperature, and Arg-CGAC showed a more favorable ΔG° than CGAC, indicating that Arg-CGAC adsorption is more favorable at higher temperatures. Thus, 323 K was identified as the most energy-efficient temperature for Pb^{2+} adsorption onto both adsorbents. These findings suggest that arginine modification significantly enhances the adsorption capacity for Pb^{2+} adsorption.

3.6 Comparison of different agricultural waste materials for Pb^{2+} removal

There are many agricultural waste materials prepared modified and unmodified AC designed for Pb^{2+} ions removal in the reference, from which the representative materials that can remove Pb^{2+} ions from waste water were chosen for comparison with CGAC and Arg-CGAC as shown in Table 5. Arg-CGAC possessed the advantage mainly on the adsorption capacities. This finding result has the same trend as some other results in which the arginine modification and CGAC have influence on the removal of Pb^{2+}. The modification of activated carbon by adding arginine has proven to be an effective strategy for

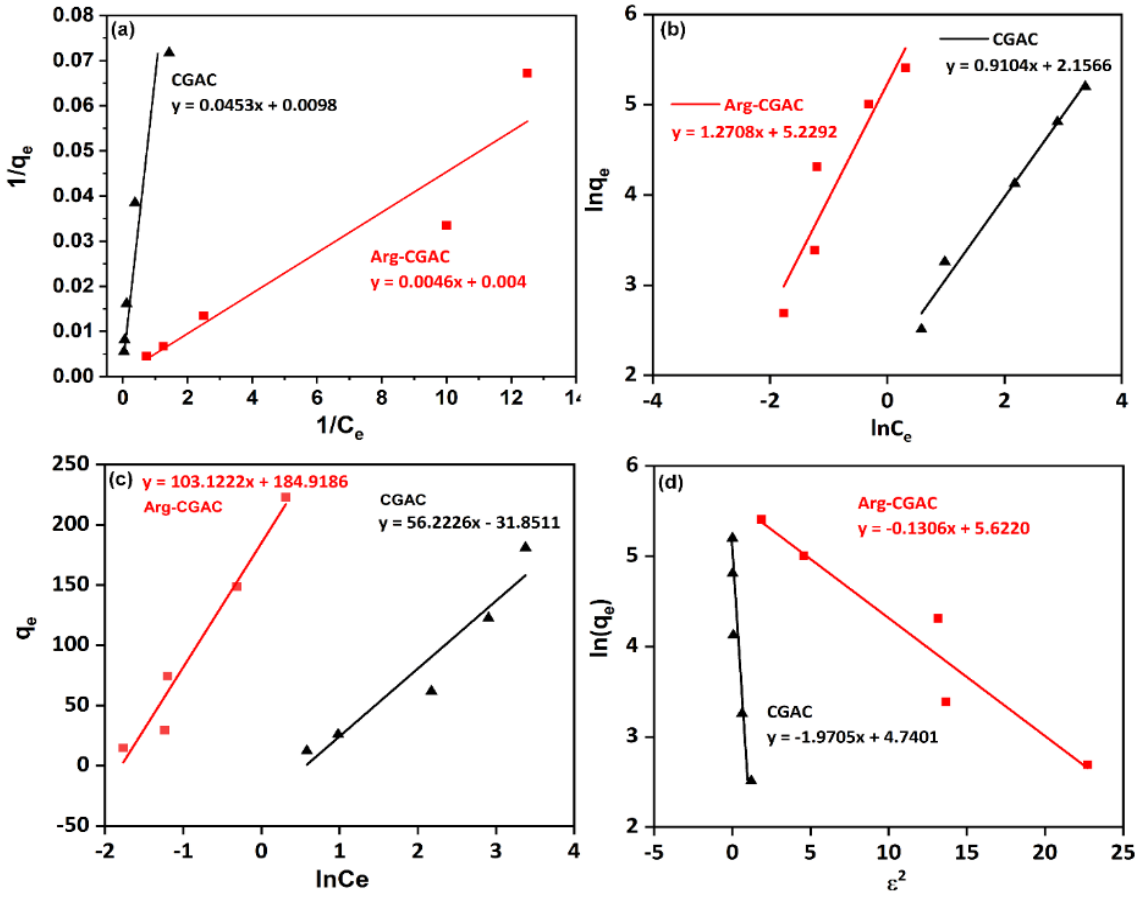

Figure 5. Isotherm plots of (a) Langmuir, (b), Freundlich, (c) Temkin and (d) Dubinin–Radushkevich models on Pb^{2+} adsorption capacity by CGAC and Arg-CGAC adsorbents.

enhancing Pb^{2+} adsorption. The unique properties of arginine, particularly its guanidino group, make it the good choice for functionalization compared to other [20]. The positively charged guanidino group in arginine can interact with negatively charged Pb^{2+} ions, enhancing the adsorption process. Additionally, this modification may also help in achieving stable binding and improving the durability of the adsorbent in long-term use [21,30]. Therefore, it is suitable for practical applications in industry and water treatment.

3.7 Reusability of CGAC and Arg-CGAC

Reusability is a key factor in assessing an adsorbent's efficiency. The reusability of CGAC and Arg-CGAC was evaluated after regeneration by elution. The adsorbents were subjected to five adsorption-desorption cycles to assess their performance over repeated use. For desorption, an ethanol-water mixture (70:30 v/v) was used as the eluent to remove adsorbed Pb^{2+} from the adsorbents. After each adsorption cycle, the spent adsorbent was thoroughly washed with distilled water, then immersed in the ethanol-water mixture and stirred for 2 h at room temperature. The desorbed adsorbent was filtered, dried at 60°C for 12 h, and reused in the subsequent adsorption cycle. The adsorption experiments in each cycle were conducted using 0.1 g of adsorbent, a Pb^{2+} solution of 150 $mg \cdot L^{-1}$, a contact time of 90 min, and a temperature of 30°C. The Pb^{2+} removal efficiencies of CGAC and Arg-CGAC over 7 reuse cycles are illustrated in Figure 6, showing their potential for regeneration and reuse. In the fourth desorption cycle, the regeneration yield exceeded 96.69% for CGAC and 97.82%. However, after the seventh cycle, the % removal decreased to below 55% and 60% for CGAC and Arg-CGAC, respectively, indicating saturation of the adsorbents. Achieving a desorption yield of 98% over 4 cycles indicates excellent regeneration efficiency of the adsorbents. This is advantageous for reusability and significantly reduces the cost of heavy metal removal processes. It also shows that the adsorbents are stable and can maintain their adsorption capacity over multiple cycles. Although desorption efficiency decreases after the 7th cycle, with adsorption capacity remaining at 55% to 60%, this is still a good result. It suggests that while the adsorbents may have limitations in regeneration, they are highly effective in the initial cycles. The drop in efficiency after the 7th cycle might indicate adsorbent saturation. However, increasing the concentration of eluents or adjusting other conditions, such as desorption time or temperature, could further improve desorption efficiency.

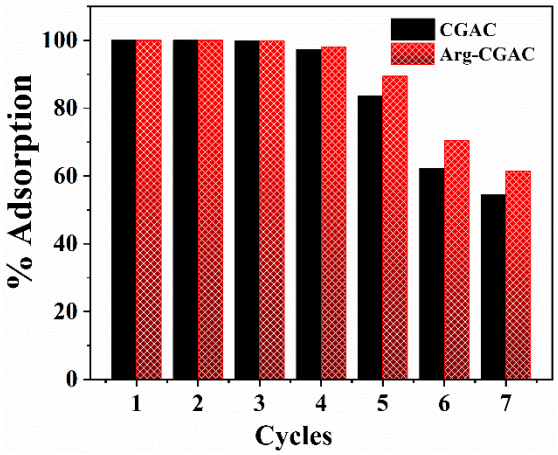

Figure 6. Reusability plots of CGAC and Arg-CGAC adsorbents on Pb^{2+} adsorption capacity.

Table 4. Thermodynamic parameters of the CGAC and Arg-CGAC adsorbents on Pb^{2+} ion.

Adsorbents	ΔH°	ΔS°	ΔG° [kJ·mol^{-1}]		
	[kJ·mol^{-1}]	[J·mol^{-1} K^{-1}]	303 K	313 K	323 K
CGAC	9.20	43.44	–3.96	–4.40	–4.83
Arg-CGAC	24.65	99.11	–5.38	–6.37	–7.37

Table 5. Adsorption capacity (q_e) of Pb^{2+} ions from different adsorbents.

ACs from various materials	Modified AC	q_e [mg·g^{-1}]	Ref.
Bagasse	-	59.35	[31]
	Nitric acid 10 M	168.30	
Parthenium hysterophorus plant	-	125.00	[32]
	Iron oxide	166.60	
Corncob	maghemite	127.00	[33]
Water hyacinth	Nitric acid 10 M	175.60	[34]
	2-aminothiazole chelating legend	310.90	
Activated carbon fibers	-	136.80	[35
	L-cysteine	179.53	
Activated carbon	Sulfhydryl	116.30	[36]
Sodium montmorillonite	Arginine	124.69	[30]
Carbon nanotubes	selenophosphoryl groups	156.25	[37]
Coffee grounds	-	67.04	[17]
Coffee grounds	sodium alginate bead	57.91	[38]
Coffee grounds	-	199.23	This study
	Arginine	223.10	

4. Conclusion

The maximum adsorption capacities at equilibrium (q_e) for Pb^{2+} at an initial concentration of 150 $mg \cdot L^{-1}$, contact time of 90 min, temperature of 30°C, and a dose of 0.1 g were 119.23 $mg \cdot g^{-1}$ for CGAC and 223.10 $mg \cdot g^{-1}$ for Arg-CGAC. Isotherm analysis suggests that Arg-CGAC has a higher adsorption capacity, stronger adsorbate-adsorbent interactions, and a more endothermic adsorption process compared to CGAC. Arg-CGAC exhibited both physisorption and weak chemisorption, while CGAC primarily showed physisorption. The Freundlich and Temkin isotherms best fit both adsorbents, with Arg-CGAC displaying a particularly strong affinity for Pb^{2+}. The $\Delta G°$ values became more negative with increasing temperature, indicating more favorable adsorption at higher temperatures, especially for Arg-CGAC. The most energy-efficient temperature for Pb^{2+} adsorption was identified as 323 K. Arginine modification significantly enhanced Pb^{2+} adsorption capacity. A desorption yield of 98% was achieved over 4 cycles, though efficiency declined after the 7th cycle, with adsorption capacity stabilizing at 55% to 60%, indicating good performance in the initial cycles despite some regeneration limitations.

Acknowledgements

This work was funded by National Higher Education, Science, Research and Innovation Policy Council, Thaksin University (Research project grant) Fiscal Year 2022, Thailand. We sincerely acknowledge for the partial financial support by Thaksin University Research Fund.

References

[1] O. Alam, and X. Qiao, "Influences of chemically controlled Ca-bearing minerals in chitosan on P^{b2+} removal efficiency," *Journal of Environmental Health Science and Engineering,* vol. 18, no. 2, pp. 993-1005, 2020.

[2] O. Alam, X. J. Zheng, D. Du, X. Qiao, L. Dai, J.. Li, J. Xia, J. Ye, and S. Zhong, "A critical review on advances in remediation of toxic heavy metals contaminated solids by chemical processes," *Journal of Environmental Chemical Engineering,* vol. 12, no. 4, p. 113149, 2024.

[3] I. Ali, C. Peng, D. Lin, D. P. Saroj, I. Naz, Z. M. Khan, M. Sultan, and M. Ali, "Encapsulated green magnetic nanoparticles for the removal of toxic Pb^{2+} and Cd^{2+} from water: Development, characterization and application," *Journal of Environmental Management,* vol. 234, no. 2019, pp. 273-289, 2019.

[4] G. Murtaza, A. Ditta, N. Ullah, M. Usman, and Z. Ahmed, "Biochar for the management of nutrient impoverished and metal contaminated soils: preparation, applications, and prospects," *Journal of Soil Science and Plant Nutrition,* vol. 21, no. 3, pp. 2191-2213, 2021.

[5] S. Bahah, "Analytical study on lead elimination by anionic clays: Characterization, adsorption kinetics, isotherm, thermo-dynamic, mechanism and adsorption," *Analytical Methods in Environmental Chemistry Journal,* vol. 6, no. 3, pp. 67-88, 2023.

[6] O. Uygun, A. Murat, and G. O. Çakal, "A novel magnetic sepiolite/Fe_2O_3 composite for adsorptive removal of lead(II) ions from aqueous solutions," *Clay Minerals,* vol. 58, no. 3, pp. 1-32, 2023.

[7] A. El Mouden, N. El Messaoudi, A. El Guerrak, A. Bouich, V. Mehmeti, A. Lacherai, A. Jada, and J. H. P. Americo-Pinheiro, "Removal of cadmium and lead ions from aqueous solutions by novel dolomite-quartz@Fe_3O_4 nanocomposite fabricated as nanoadsorbent," *Environmental Research,* vol. 225, no. 2022, p. 115606, 2023.

[8] C. Shao, F. Fan, and Y. Dai, "Lead ions removal from water by tartaric acid modified biochar materials: Equilibrium, kinetic studies and mechanism," *Desalination and Water Treatment,* vol. 320, p. 100601, 2024.

[9] P. Kongsune, S. Rattanapan, and R. Chanajaree, "The removal of Pb^{2+} from aqueous solution using mangosteen peel activated carbon: Isotherm, kinetic, thermodynamic and binding energy calculation," *Groundwater for Sustainable Development,* vol. 12, p. 100524, 2021.

[10] S. Rattanapan, J. Srikram, and P. Kongsune, "Adsorption of methyl orange on coffee grounds activated carbon," *Energy Procedia,* vol. 138, pp. 949-954, 2017.

[11] S. Rattanaphan, T. Rungrotmongkol, and P. Kongsune, "Biogas improving by adsorption of CO_2 on modified waste tea activated carbon," *Renewable Energy,* vol. 145, pp. 622-631, 2020.

[12] D. Khater, M. Alkhabbas, and A. M. Al-Ma'abreh, "Adsorption of Pb, Cu, and Ni ions on activated carbon prepared from oak cupules: Kinetics and thermodynamics studies," *Molecules,* vol. 29, no. 11, p. 2489, 2024.

[13] M. S. Hossen, T. Islam, S. M. Hoque, A. Islam, M. M. Bashar, and G. Bhat, "Synthesis, activation, and characterization of carbon fiber precursor derived from jute fiber," *ACS Omega,* vol. 9, no. 33, pp. 35384-35393, 2024.

[14] M. C. Silva, L. H. S. Crespo, A. L. Cazetta, T. L. Silva, L. Spessato, and V. C. Almeida, "Activated carbon fibers of high surface area from corn husk: Mono and multicomponent adsorption studies of Pb^{2+} and Cu^{2+} ions from aqueous solution," *Journal of Molecular Liquids,* vol. 405, no. 2023, p. 124919, 2024.

[15] R. Campbell, B. Xiao, and C. Mangwandi, "Production of activated carbon from spent coffee grounds (SCG) for removal of hexavalent chromium from synthetic wastewater solutions," *Journal of Environmental Management*, vol. 366, p. 121682, 2024.

[16] V. E. Pakade, L. M. Madikizela, M. J. Klink, and S. Ncube, "Adsorption of toxic heavy metals using charred and uncharred coffee waste adsorbents: a review," *Environmental Technology Reviews,* vol. 12, no. 1, pp. 359-389, 2023.

[17] J. Chen, Y. Liu, J. Liu, Q. Duan, Z. Wang, J. Song, C. Ji, and J. Sun, "Effects of carbonization on the structure and sorption properties of coffee grounds for Pb(II) and Ni(II) in various metal systems," *Desalination and Water Treatment,* vol. 320, no. 9, p. 100623, 2024.

[18] X. Yang, Y. Wan, Y. Zheng, F. He, Z. Yu, J. Huang, H. Wang, Y. S. Ok, Y. Jiang, and B. Gao, "Surface functional groups of carbon-based adsorbents and their roles in the removal of heavy

metals from aqueous solutions: A critical review," (in eng), *Chemical Engineering Journal,* vol. 366, pp. 608-621, 2019.

[19] B. Liu, P. Lv, Q. Wang, Y. Bai, J. Wang, W. Su, X. Song, and G. Yu, "Statistical physics investigation on the simultaneous adsorption mechanism of Cd^{2+} and Pb^{2+} on amino functionalized activated carbon derived from coal gasification fine slag," *Journal of Environmental Chemical Engineering,* vol. 12, no. 3, p. 112635. 2024.

[20] M. Naushad, A. A. Alqadami, Z. A. AlOthman, I. H. Alsohaimi, M. S. Algamdi, and A. M. Aldawsari, "Adsorption kinetics, isotherm and reusability studies for the removal of cationic dye from aqueous medium using arginine modified activated carbon," *Journal of Molecular Liquids,* vol. 293, p. 111442, 2019.

[21] C. Zhang, S. Qi, J. Meng, and X. Chen, "Selective and efficient extraction of heparin by arginine-functionalized flowered mesoporous silica nanoparticles with high capacity," *Separation and Purification Technology,* vol. 276, p. 119321, 2021.

[22] W. Liu, J. Zhang, Y. Jin, X. Zhao, and Z. Cai, "Adsorption of Pb(II), Cd(II) and Zn(II) by extracellular polymeric substances extracted from aerobic granular sludge: Efficiency of protein," *Journal of Environmental Chemical Engineering,* vol. 3, no. 2, pp. 1223-1232, 2015.

[23] L. Brini, A. Hsini, Y. Naciri, A. Bouziani, Z. Ajmal, K. H' Maida, A. Boulahya, M. Arahou, B. Bakiz, A. Albourine, and F. Mohamed, "Synthesis and characterization of arginine-doped heliotrope leaves with high clean-up capacity for crystal violet dye from aqueous media," *Water Science and Technology,* vol. 84, no. 9, pp. 2265-2277, 2021.

[24] S. Brunauer, P. H. Emmett, and E. Teller, "Adsorption of gases in multimolecular layers," *Journal of The American Chemical Society,* vol. 60, no. 2, pp. 309-319, 1938.

[25] N. Nikolić, V. Maksimovic, and A. Ljiljana, "Correlation of morphology and crystal structure of metal powders produced by electrolysis processes," *Metals,* vol. 11, p. 859, 2021.

[26] I. Langmuir, "The adsorption of gases on plane surfaces of glass, mica, and platinum," *Journal of the American Chemical Society,* vol. 40, pp. 1361-1403, 1918.

[27] H. M. F. Freundlich, "Over the Adsorption in Solution," *The Journal of Physical Chemistry,* vol. 57, pp. 385-470, 1906.

[28] M. J. Temkin, and V. Pyzhev, "Recent modifications to langmuir isotherms," *Acta Physiochim U.R.S.S,* vol. 12, pp. 217-225, 1940.

[29] M. M. Dubinin, and L. V. Radushkevich, "The equation of the characteristic curve of the activated charcoal," *Proceedings of the Academy of Sciences of the USSR. Physical chemistry section*, vol. 55, pp. 331-337, 1947.

[30] Y. Chu, M. A. Khan, F. Wang, M. Xia, W. Lei, and S. Zhu, "Kinetics and equilibrium isotherms of adsorption of Pb(II) and Cu(II) onto raw and arginine-modified montmorillonite," *Advanced Powder Technology,* vol. 30, no. 5, pp. 1067-1078, 2019.

[31] W. Somyanonthanakun, R. Ahmed, V. Krongtong, and S. Thongmee, "Studies on the adsorption of Pb(II) from aqueous solutions using sugarcane bagasse-based modified activated carbon with nitric acid: Kinetic, isotherm and desorption," *Chemical Physics Impact,* vol. 6, p. 100181, 2023.

[32] A. Rehman, A. Naeem, I. Ahmad, D. Fozia, B. Almutairi, M. Aslam, M. Israr, B. O. Almutairi, and Z. Ullah, "Synthesis of plant-mediated iron oxide nanoparticles and optimization of chemically modified activated carbon adsorbents for removal of As, Pb, and Cd ions from wastewater," *ACS Omega,* vol. 9, no. 1, pp. 317-329, 2024.

[33] A. Arul, S. Kavitha, A. Anand Babu Christus, V. J. Surya, A. Ravikumar, and Y. Sivalingam, "Enhanced removal of Pb (II) and Cd (II) ions from aqueous systems using coated magnetic nanoparticles in activated carbon derived from corncob waste," *Surfaces and Interfaces,* vol. 40, p. 103095, 2023.

[34] S. M. Waly, A. M. El-Wakil, W. M. A. El-Maaty, and F. S. Awad, "Efficient removal of Pb(II) and Hg(II) ions from aqueous solution by amine and thiol modified activated carbon," *Journal of Saudi Chemical Society,* vol. 25, no. 8, p. 101296, 2021.

[35] L. Zhu, Y. Yao, D. Chen, and P. Lan, "The effective removal of Pb^{2+} by activated carbon fibers modified by l-cysteine: exploration of kinetics, thermodynamics and mechanism," *RSC Advances,* vol. 12, no. 31, pp. 20062-20073, 2022.

[36] M. S. Alhumaimess, "Sulfhydryl functionalized activated carbon for Pb(II) ions removal: kinetics, isotherms, and mechanism," *Separation Science and Technology,* vol. 55, no. 7, pp. 1303-1316, 2020.

[37] J. Kończyk, S. Żarska, and W. Ciesielski, "Adsorptive removal of Pb(II) ions from aqueous solutions by multi-walled carbon nanotubes functionalised by selenophosphoryl groups: Kinetic, mechanism, and thermodynamic studies," *Colloids and Surfaces A: Physicochemical and Engineering Aspects,* vol. 575, pp. 271-282, 2019.

[38] H. M. Alraddadi, T. M. Fagieh, E. M. Bakhsh, K. Akhtar, S. B. Khan, S. A. Khan, E. A. Bahaidarah, and T. A. Homdi, "Adsorptive removal of heavy metals and organic dyes by sodium alginate/coffee waste composite hydrogel," *International Journal of Biological Macromolecules,* vol. 247, p. 125708, 2023.